IEEE Access
Multidisciplinary : Rapid Review : Open Access Journal

Received January 14, 2019, accepted January 25, 2019, date of publication January 29, 2019, date of current version February 14, 2019.

Digital Object Identifier 10.1109/ACCESS.2019.2895999

Long-Term Operational Data Analysis of an In-Service Wind Turbine DFIG

ESTEFANIA ARTIGAO[1], ANGEL SAPENA-BANO[2], ANDRÉS HONRUBIA-ESCRIBANO[1], JAVIER MARTINEZ-ROMAN[2], (Member, IEEE), RUBEN PUCHE-PANADERO[2], (Member, IEEE), AND EMILIO GÓMEZ-LÁZARO[1], (Senior Member, IEEE)

[1]DIEEAC-ETSII, Renewable Energy Research Institute, University of Castilla–La Mancha, Campus Universitario, 02071 Albacete, Spain
[2]Institute for Energy Engineering, Universitat Politècnica de València, 46022 Valencia, Spain

Corresponding author: Estefania Artigao (estefania.artigao@uclm.es)

This work was supported in part by the Agreement signed between the UCLM and the Council of Albacete to promote research in the Campus of Albacete, and in part by the European Union Horizon 2020 Research and Innovation Programme through the Marie Sklodowska-Curie Grant (AWESOME Project) under Grant 642108.

ABSTRACT While wind turbine (WT) power capacities continue to increase and new offshore developments are being deployed, operation and maintenance (O&M) costs continue to rise, becoming the center of attention in the wind energy sector. The electric generator is among the top three contributors to failure rates and downtime of WTs, where the doubly fed induction generator (DFIG) is the dominant technology among variable speed WTs. Thus, the early detection of generator faults, which can be achieved through predictive maintenance, is vital in order to reduce O&M costs. The goal of this paper is to analyze a long-term monitoring campaign of an in-service WT equipped with a DFIG. A novel method named the harmonic order tracking analysis is used with two main objectives: first, to facilitate the data interpretation for non-trained maintenance personnel, and second, to reduce the amount of data that must be stored and transferred for the diagnosis of the DFIG. This method is applied and validated for the first time on an operating WT.

INDEX TERMS Condition monitoring, current signature analysis, DFIG, HOTA, wind turbine.

ACRONYMS

AS	Analytic Signal
CBM	Condition-Based Maintenance
CM	Condition Monitoring
CMS	Condition Monitoring System
CSA	Current Signature Analysis
DFIG	Doubly-Fed Induction Generator
DWT	Discrete Wavelet Transform
EPV	Extended Park's Vector
FBM	Failure-Based Maintenance
FFT	Fast Fourier Transform
HOTA	Harmonic Order Tracking Analysis
HT	Hilbert Transform
IF	Instantaneous Frequency
IM	Induction Machine
LSH	Lower Side-band Harmonic
O&M	Operation and Maintenance
PMSM	Permanent Magnet Synchronous Machine
TBM	Time-Based Maintenance
USH	Upper Side-band Harmonic
WRIM	Wound Rotor Induction Machine
WT	Wind Turbine

The associate editor coordinating the review of this manuscript and approving it for publication was Ton Do.

I. INTRODUCTION

Wind power generation had achieved 539.6 GW of global cumulative installed capacity by the end of 2017, 18.8 GW of which was located offshore [1]. The continuous and rapid growth of wind turbine (WT) power capacities [2]–[4] has generated significant challenges to be addressed with regard to operation and maintenance (O&M) strategies and costs. These represent 25% of the total expenditure of a wind farm project for onshore sites [5], which rises to 35% offshore [6]. Larger WTs have been shown to develop more faults than smaller ones [7], [8], while offshore sites can be inaccessible for long periods of time, and access is more expensive [9], [10]. All this, together with the fact that a significant share of the European wind turbine fleet is reaching the end of its expected 20-year lifetime, has made the O&M of WTs a critical issue [11], [12].

Three maintenance strategies are commonly implemented for WTs: time-based maintenance (TBM), failure-based maintenance (FBM), and condition-based maintenance (CBM). Recent trends are shifting from TBM and FBM towards CBM [13]–[15], where condition monitoring (CM) determines the optimum point between scheduled and corrective actions [16], [17]. Thus, unnecessary repair actions and unplanned downtime are reduced, in turn improving reliability and availability of WTs while reducing costs.

The electric generator is among the top three contributors to WT failure rates and downtime [18], [19], where the doubly-fed induction generator (DFIG) is the dominant technology in variable-speed WTs [20], [21]. CM on this WT component is therefore key to achieving higher availabilities while reducing O&M costs. Commercially available condition monitoring system (CMS), however, are commonly based on vibrations and target the drive train (mainly gearbox and bearings [22], [23]), failing to provide the health status of the electric generator. Various techniques have been proposed in the scientific literature as a means for fault detection of electric generators, with current signature analysis (CSA) being highlighted as the preferred option [24], [25] due to its detection capabilities (both electrical and mechanical related faults) and low cost.

Operational data on in-service WT generators are rarely presented in the scientific literature. More specifically, only four publications have been found for CSA applied to in-service WT DFIGs [26]–[29]. The analysis of the DFIG used for the present work was provided in [26], being diagnosed with mixed eccentricity by the authors of the present study. In [27], high-speed shaft unbalance was detected using CSA. Zhang and Neti [28] and Cheng *et al.* [29] detected gearbox bearing faults using the stator currents of the DFIG. In three of these publications, the number of measurements and working conditions analyzed is limited to a maximum of six measurements and three working conditions only. Although Cheng *et al.* [29] presented an averaged representation of a greater number of measurements, these were gathered over a short period. The analysis of field measurements of operating WT DFIGs involves further difficulties compared to laboratory-based experiments, since operating conditions or external factors (extreme weather) cannot be controlled or replicated. All these factors highlight the need to develop further analyses of WT DFIGs operating in the field.

Moreover, all four of the above-mentioned studies required specialized personnel to interpret the results obtained by CSA. In order to overcome this limitation, the novel method named Harmonic Order Tracking Analysis (HOTA) is used in the present work to analyze data from an in-service WT DFIG over a period of eight months. The HOTA method was first presented in [30] by the authors of the present paper and further developed in subsequent studies, at laboratory scale. The present work thus contributes to validating the HOTA method for wind power applications. For the first time in the scientific literature, large amount of operational data are analyzed over a long period of time, being easily rendered and requiring reduced data storage.

In addition to this introduction, the paper is structured as follows: in section II, the data used for the analysis are presented. Section III describes the HOTA method. The steps followed to apply the HOTA method to the operational data are described in section IV. The results and the validation of the proposed method are presented in section V. The advantages of HOTA compared to traditional methods, as well as further capabilities of HOTA, are illustrated in section VI. Finally, the conclusions drawn from the various analyses are summarized in section VII.

II. IN-SERVICE WT DATA USED FOR THE ANALYSIS

The WT under analysis is an 850 kW nominal power, 2 pole pair DFIG diagnosed with mixed eccentricity [26]. The data used for the present analysis comprise 3-phase rotor and stator current signals collected over a period of eight months of WT operation. The location of the current sensors within the WT drive train is depicted in Fig. 1. The types of current measurements used for the present work are summarized in Table 1. These data were extracted from a database owned by the Spanish company Ingeteam Power Technology S.A. UP Service (located in Albacete, Spain). Ingeteam specializes in Condition Monitoring Systems and SCADA Systems, as well as power converters, generators and turbine controllers. They have equipped 40 GW of wind power worldwide, 12 GW of which corresponds to O&M activities (covering more than 5,600 wind turbines).

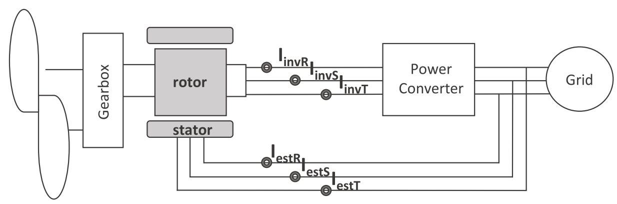

FIGURE 1. DFIG Diagram with location of current sensors.

TABLE 1. Type of signals used for the analysis.

Label	Sensor Location	Sampling Parameters
I_{est}	stator current phase a stator current phase b stator current phase c	1.5 kHz 5.4 s
I_{inv}	rotor-side converter current phase a rotor-side converter current phase b rotor-side converter current phase c	

The data acquired for each month ranged from over 300 to 900 files per month, comprising a total of 5,834 files for the whole monitoring campaign. The data were gathered using different triggers, described as follows. There were three triggers based on an increment in the current rms, and two periodic triggers. The first three occur when the current exceeds:

1) 630 A (i.e. rise in load over 75%).
2) 500 A (i.e. rise in load over 60%).
3) 300 A (connected, approximately 45% of the generator load).

The two periodic triggers occur:

1) After 15 h of no-acquisition.
2) When any of the previous conditions are met for more than one hour.

In the present work, spectral analysis, which relies on the signal being stationary, was performed. For this reason, the first step was to discriminate between permanent and transient regime signals, where the signals not meeting stationary conditions were rejected. The criteria used to discriminate between permanent and transient regimes is explained as follows. Each measurement was divided into eight parts, and the following parameters were calculated for each of the eight parts, for each of the three phases:

- RMS value of raw stator currents.
- Mains frequency of stator currents.
- RMS value of raw rotor-side converter currents.
- Mains frequency of rotor-side converter currents.

When the mains frequencies of the stator and rotor-side currents remained constant, and the differences between the RMS values of the stator and rotor-side currents were lower than 10%, the measurement was considered stationary.

The second step was to categorize the remaining signals per speed range of the high-speed shaft, where *High* includes the measurements obtained for rotational speeds over 1,500 rpm (of the high-speed shaft), *Med* for rotational speeds between 1,250 and 1,500 rpm, and *Low* for rotational speeds below 1,250 rpm. The number of files per month and files per speed range used are summarized in Table 2.

TABLE 2. Summary of the monthly data used.

Month	No. of measurements	Speed range [rpm]	No. of files at condition
November 2015	212	High	101
		Med	50
		Low	61
December 2015	82	High	17
		Med	25
		Low	40
January 2016	259	High	174
		Med	39
		Low	46
February 2016	164	High	86
		Med	24
		Low	54
March 2016	180	High	83
		Med	43
		Low	54
April 2016	96	High	24
		Med	30
		Low	42
May 2016	160	High	30
		Med	51
		Low	79
June 2016	132	High	45
		Med	35
		Low	52
TOTAL	1,285	High	560
		Med	297
		Low	428

III. THE HARMONIC ORDER TRACKING ANALYSIS (HOTA) METHOD

CSA methods are based on the fact that each type of fault introduces or amplifies different harmonic components in both the stator and the rotor currents. In the case of a mixed eccentricity fault, the amplitude of the stator and rotor current harmonics of frequencies given by (1) and (2), respectively, are modified [31]:

$$f_{ecc}^{s} = f_1 \pm k f_r, \quad k = 1, 2, 3 \ldots \tag{1}$$

$$f_{ecc}^{r} = s f_1 \pm k f_r, \quad k = 1, 2, 3 \ldots \tag{2}$$

where f_1 is the power supply frequency, s is the slip, f_r the mechanical rotational speed of the machine, and k the harmonic order.

Needless to say, not only the method used for CM but also the location (steady state regime) or evolution (transient regime) of the fault harmonic components depend on the working condition. In Fig. 2 a), the conventional spectrum of two rotor currents of the DFIG working at sub- and super-synchronous speeds is shown in blue and red, respectively. As can be seen, not only the rotor mains frequency, but also the fault harmonic components appear at different frequencies for different working conditions. Therefore, further individual analyses are required for each spectrum to evaluate whether the harmonic components found are due to a fault or not, and if the amplitude is high enough to be considered a fault. Highly specialized maintenance personnel are thus needed to calculate and determine the condition of the machine using traditional CSA. The analysis is even more complex for transient regimes in terms of memory, computing power and interpretation of the results, requiring more advanced signal processing methods. Moreover, in the case of operating WT DFIGs, the amount of data to be sent to the control center is usually limited, which may limit the application of CSA in the field.

The HOTA method was developed to address the above-mentioned problems. HOTA was first presented in [30] to diagnose induction machine (IM)s working under steady-state regime, and later extended in [32] for IMs working under non-stationary conditions. However, like most of the traditional stator CSA methods, the aforementioned versions of HOTA require information about the IM's rotational speed. Nevertheless, such measurement may be avoided by analyzing the rotor currents, as proven in [33] and [34]. For that reason, in [35], HOTA was adapted to the analysis of the rotor currents and applied to a wound rotor induction machine (WRIM) working under non-stationary conditions, avoiding the need to measure the IM's rotational speed.

TABLE 3. Statistical results for the harmonic orders $k = \pm 1$ of the whole data set processed using HOTA per speed regime.

DATA No. of signals analyzed		Total 1,285	$n \leq 1,250$ rpm 427	$1,250 < n < 1,500$ rpm 298	$n \geq 1,500$ rpm 560
$k = -1$	Upper adjacent (dB)	−27.74	−27.74	−28.22	−32.43
	75th percentile (dB)	−30.60	−29.51	−30.12	−34.29
	Median (dB)	−32.44	−30.67	−31.11	−34.97
	25th percentile (dB)	−34.84	−31.40	−32.23	−35.58
	Lower adjacent (dB)	−38.07	−32.96	−34.93	−37.05
	Outliers	6	6	0	4
	Dispersion |Upper-Lower| (dB)	10.33	5.22	6.71	4.62
$k = +1$	Upper adjacent (dB)	−23.46	−21.20	−30.87	−34.85
	75th percentile (dB)	−31.59	−26.19	−32.40	−36.55
	Median (dB)	−33.64	−30.53	−33.17	−37.18
	25th percentile (dB)	−37.03	−31.79	−33.66	−37.83
	Lower adjacent (dB)	−39.64	−33.94	−35.40	−39.64
	Outliers	16	0	2	3
	Dispersion |Upper-Lower| (dB)	16.18	12.74	4.53	4.79

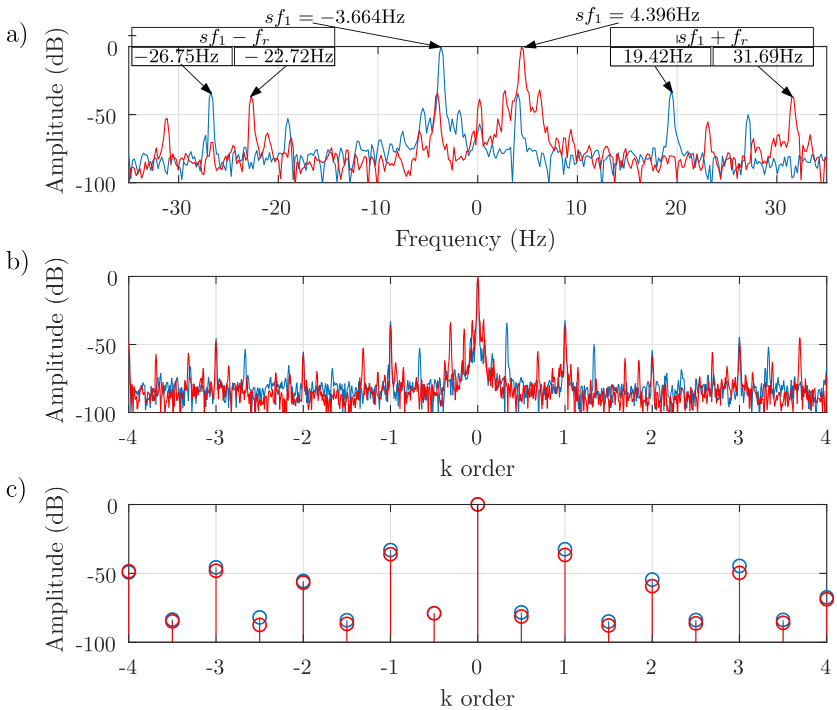

FIGURE 2. Graphical visualization of the HOTA method. *a*) Spectrum of two rotor current measurements. *b*) First step in HOTA, the frequency axis is transformed into harmonic order values. *c*) Second step in HOTA, the relevant data set.

HOTA proposes a transformation of the frequency axis in the three dimensional spectograms (for transient regimes) or in the conventional spectrum (for steady-state regime) in terms of the harmonic order k in (1) and (2). In this way, a new representation is achieved, whose appearance is similar to a conventional spectrum, but the fault harmonic components are always located in the same positions (at k integer values of the given fault) regardless of the frequency supply or rotational speed. This is shown in Fig. 2 b). As a result, the interpretation of the diagnostic results becomes simpler, eliminating the need for specialized maintenance personnel. Furthermore, since the fault harmonic components are always located at the same positions, the maintenance personnel do not require additional information about the WT working condition and only the amplitudes of the fault harmonic components have to be compared with the thresholds for each fault, which do not generally involve any specific knowledge or specialization. In fact, the use of a color code depending on the thresholds can facilitate this task.

In a second step, HOTA proposes reducing the memory storage and transmission capabilities by reducing the number of data points needed for diagnostic purposes. In this regard, only the amplitudes of the fault harmonic components and the level of the spectral noise (less than 20 real numbers) are needed, as per Fig. 2 c). Hence, HOTA proposes to save and transfer these values only in order to track the evolution of the machine's condition.

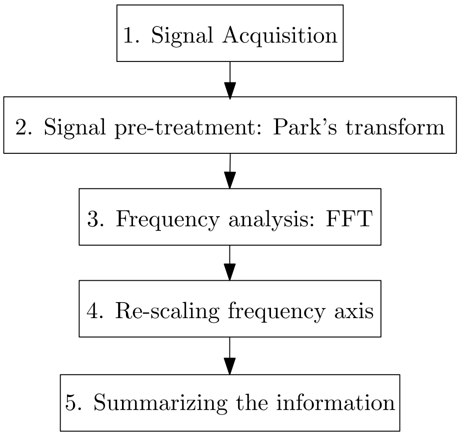

FIGURE 3. Block diagram of HOTA to be applied to the WT working under steady-state regime.

IV. APPLICATION OF HOTA TO A LARGE VOLUME OF DATA

In order to apply the HOTA method to the eight-month data of the operating WT DFIG under study, the method is decomposed into five conceptual tasks, shown in Fig. 3 and explained as follows.

1) Signal Acquisition. The rotor-side converter currents are acquired for each phase (a, b, c).
2) Signal pre-treatment: Park's transform. The direct, i_{d_r}, and the quadrature, i_{q_r}, components of the Park's transform of the three mentioned currents (i_{a_r}, i_{b_r} and i_{c_r}) are computed as [36]:

$$i_{d_r}(t) = \sqrt{\frac{2}{3}} i_{a_r}(t) - \frac{1}{\sqrt{6}} i_{b_r}(t) - \frac{1}{\sqrt{6}} i_{c_r}(t) \quad (3)$$

$$i_{q_r}(t) = \frac{1}{\sqrt{2}} i_{b_r}(t) + \frac{1}{\sqrt{2}} i_{c_r}(t) \quad (4)$$

3) Frequency analysis via fast Fourier transform (FFT). Once the rotor's Park vector is obtained, HOTA computes the FFT spectrum as in conventional CSA methods. This step is only valid for steady-state measurements. For transient measurements, other versions of HOTA should be used, as in [32] and [35].

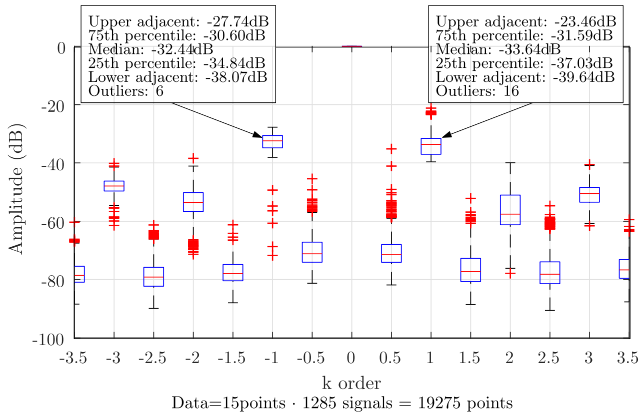

FIGURE 4. Results of HOTA applied to the DFIG under study using a box-plot.

4) Re-scaling frequency axis. Fault harmonic components related to mixed eccentricity appear in the rotor currents of the DFIG under study at frequencies given by (2). Accordingly, the frequency axis of the rotor current spectrum is re-scaled as:

$$f^T = \frac{f - f^r}{f_r} \quad (5)$$

where f^T is the transformed frequency, f is the frequency axis, and f^r is the rotor mains frequency ($f^r = sf_1$). This transformation (f^T) shifts (to a distance $f^r = sf_1$) and normalizes (by f_r) the frequency axis so that each fault harmonic component falls at integer values of k in (2). Hence the transformed frequency of a fault component of harmonic k in (2) is:

$$f^T_{kecc} = \frac{(sf_1 + kf_r) - sf_1}{f_r} = k \quad k = \pm 1, \pm 2 \ldots \quad (6)$$

As previously mentioned, no extra sensors are needed to measure the mechanical rotational speed (f_r), since it can be computed from the the slip equation as:

$$s = \frac{f_1 - pf_r}{f_1} \rightarrow f_r = \frac{f_1 - sf_1}{p} \quad (7)$$

5) Summarizing the information. Once the fault-related components are located in the new frequency axis, thus always appearing at the same positions, the relevant information for diagnostic purposes is saved. HOTA stores the amplitudes of the fault harmonic components (integer values of k from $k = -3$ to $k = 3$, including the amplitude of the mains frequency) and intermediate values, corresponding to the spectral noise between fault harmonic components. This allows the user to determine if the peak value of a fault-related component is significantly higher than the spectral noise.

V. RESULTS

In this section, the eight-month operational data of the DFIG under study is analyzed using the HOTA method, following

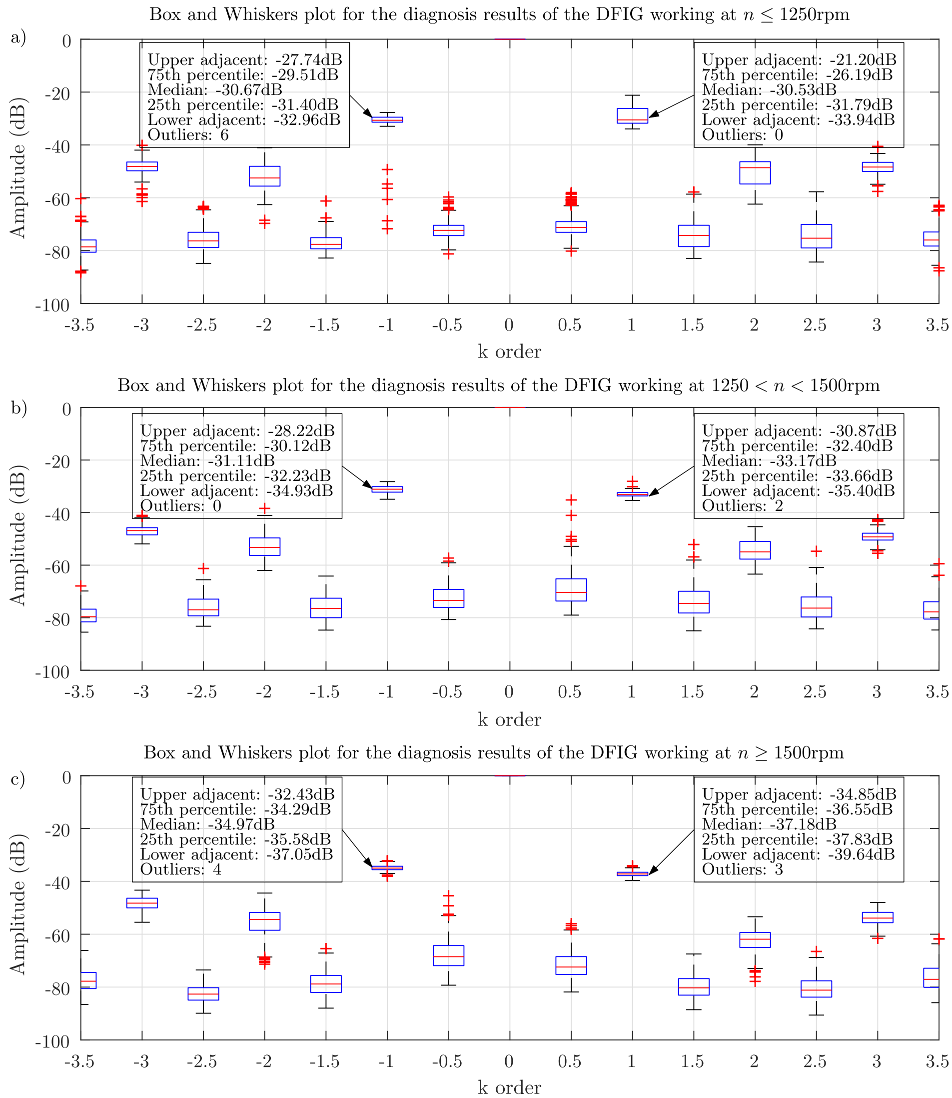

FIGURE 5. Results of HOTA applied to the DFIG under study per speed regime, *a)* $n \leq 1250$ *rpm*, *b)* $1250 < n < 1500$ *rpm* and *c)* $n \geq 1500$ *rpm*.

the steps described in section IV. With the proposed method, the information of the whole set formed by the 1,285 measurements described in section II can be displayed in a single graph, even with the DFIG operating under different loading conditions. The results are shown in Fig. 4 using a box-plot.

The central mark of each box indicates the median of the data used for the analysis. The bottom and top edges of the box indicate the 25th and 75th percentiles, respectively. The whiskers extend to the upper and lower limits belonging to the maximum and minimum values, respectively, which are not considered outliers. The outliers are plotted individually using the "+" symbol. As shown in the text boxes in Fig. 4, the fault harmonic components spread around a small band of 10.33 dB and 16.18 dB for the harmonic orders $k = -1$ and $k = +1$, respectively, providing a better insight of the state of the machine. Only 6 outliers were found for $k = -1$ and 16 for $k = +1$, which represent abnormal values of the data under analysis. Although the number of outliers is small, if these measurements were individually selected (as per traditional CSA via FFT), they would lead to an incorrect diagnosis. This highlights the improvement in the diagnostic reliability of the proposed method, where large data sets can be analyzed jointly, thus enabling easy detection of abnormalities. Since the capabilities of the HOTA method allow the analysis of large volumes of data, several types of analyses can be performed, such as historical monitoring of the evolution of the box and whiskers to detect the appearance of new faults, tracking their severity, etc.

To analyze these results quantitatively, further statistical analyses were performed classifying the measurements per rotational speed in three groups: *Low* for $n \leq 1250$ *rpm*, *Med* for $1250 < n < 1500$ *rpm*, and *High* for $n \geq 1500$ *rpm*, shown in Fig. 5. It can be clearly seen that the dispersion of each harmonic order is significantly reduced, particularly for even integer harmonics ($k = \pm 1, \pm 3$). The results for the $k = \pm 1$ harmonic orders (upper side-band harmonic (USH) and lower side-band harmonic (LSH)) are further analyzed, presented in Table 3. The USH and LSH show dispersion ranges of $<$ 6 dB and $<$ 13 dB for the *Low* speed range data points, $<$ 7 dB and $<$ 5 dB for the *Med* speed range data points, and $<$ 5 dB and $<$ 5 dB for the *High* speed range data points. It appears that the USH amplitude levels are more similar with medium and high rotational speeds.

Finally, the median and upper and lower limits are compared for each DFIG operating condition for both the LSH and USH (Fig. 6). It can be observed that the amplitude levels remain almost constant for the DFIG operating under sub-synchronous speed (*Low* and *Med* speed ranges) whereas the amplitude of the harmonic fault components decreases in the case of the DFIG operating at super-synchronous speed (*High* speed range), for the LSH. In the case of the USH, all the median and upper and lower limit levels decrease as the rotational speed increases.

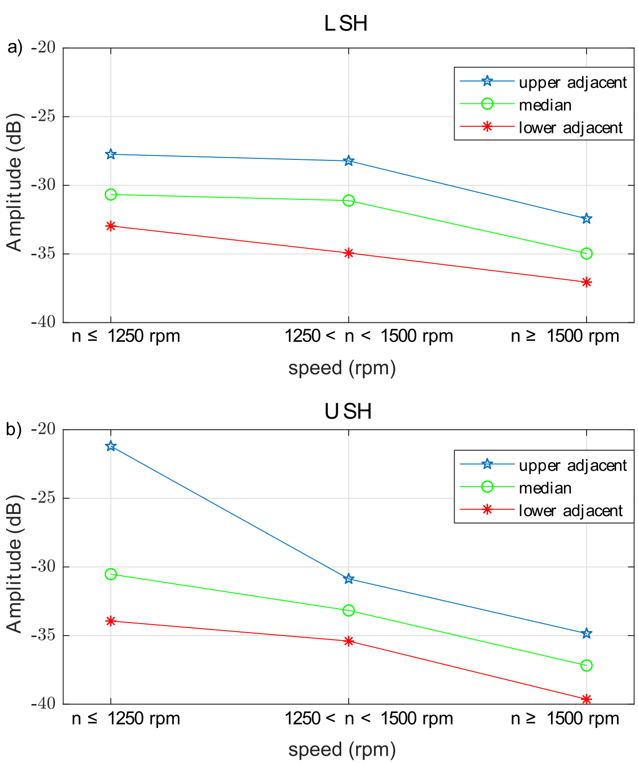

FIGURE 6. **Comparison of the median, and upper and lower limits per speed regime for *a)LSH* and *b)USH*.**

VI. DISCUSSION OF THE RESULTS

As shown in Section V, the HOTA method enables simple massive treatment of the reduced spectra, obtaining a data representation in a fast and concise manner. It also enables the statistical treatment of the data, using, for example, box plots. In this way, the amplitude levels of the fault harmonic components and their dispersion can be analyzed for the whole data set, instead of using a few selected measurements to achieve a diagnosis (as is usual in the scientific literature). The diagnostic capability is therefore improved using HOTA.

The advantages of the proposed method compared to traditional CSA via FFT applied to a large volume of data are illustrated in this section. Besides, the potential of the HOTA method towards CM is further developed, and is used to assess the influence of the loading conditions on the results.

A. ADVANTAGES OF THE HOTA METHOD COMPARED TO TRADITIONAL CSA

Fig. 7 a) and Fig. 7 b) show the rotor currents of the DFIG working at sub- and super-synchronous speeds, respectively. The spectra obtained with the conventional FFT for both measurements are plotted jointly in Fig. 7 c), where the rotor mains frequency (sf_1) and the fault harmonic components due to mixed eccentricity at the harmonic orders $k = \pm 1$ in (2) are depicted. In this way, it is necessary to locate individually for each spectrum the main component and the related fault harmonic components, which have different frequencies for each working condition. That is, since the frequencies that are relevant for diagnostic purposes will change for each measurement, with traditional CSA via FFT, the analysis of all the signals jointly is not possible, unlike in the HOTA method. This can be clearly observed comparing Fig. 2 c), with HOTA, versus Fig. 7 c), with traditional CSA, highlighting the main drawback of this traditional method.

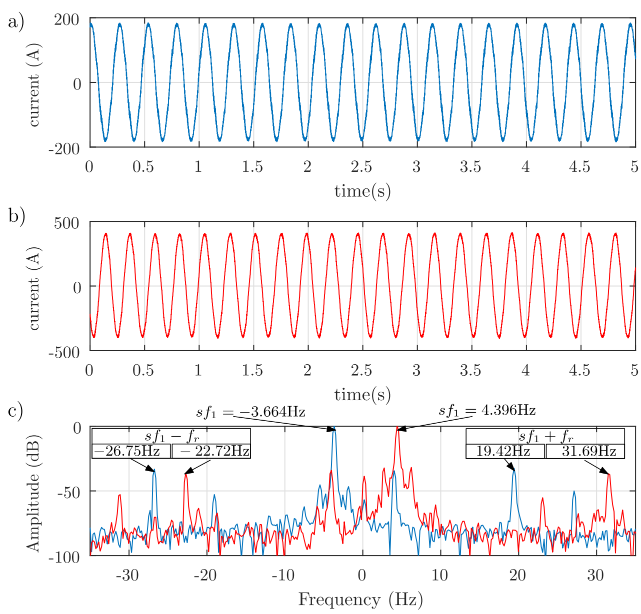

FIGURE 7. **Traditional results of CSA. *a)* Rotor current of DFIG operating at sub-synchronous speed. *b)* Rotor current of DFIG operating at super-synchronous speed. *c)* Rotor current spectra of the DFIG under both super- and sub-synchronous speeds.**

Moreover, considering that each spectrum contains $N = F_s \cdot T_{acq} = 8,100$ data points, and there are 1,285 measurements, the total quantity is $1.04 \cdot 10^7$ data points, which must be analyzed, saved and transferred. Therefore, besides

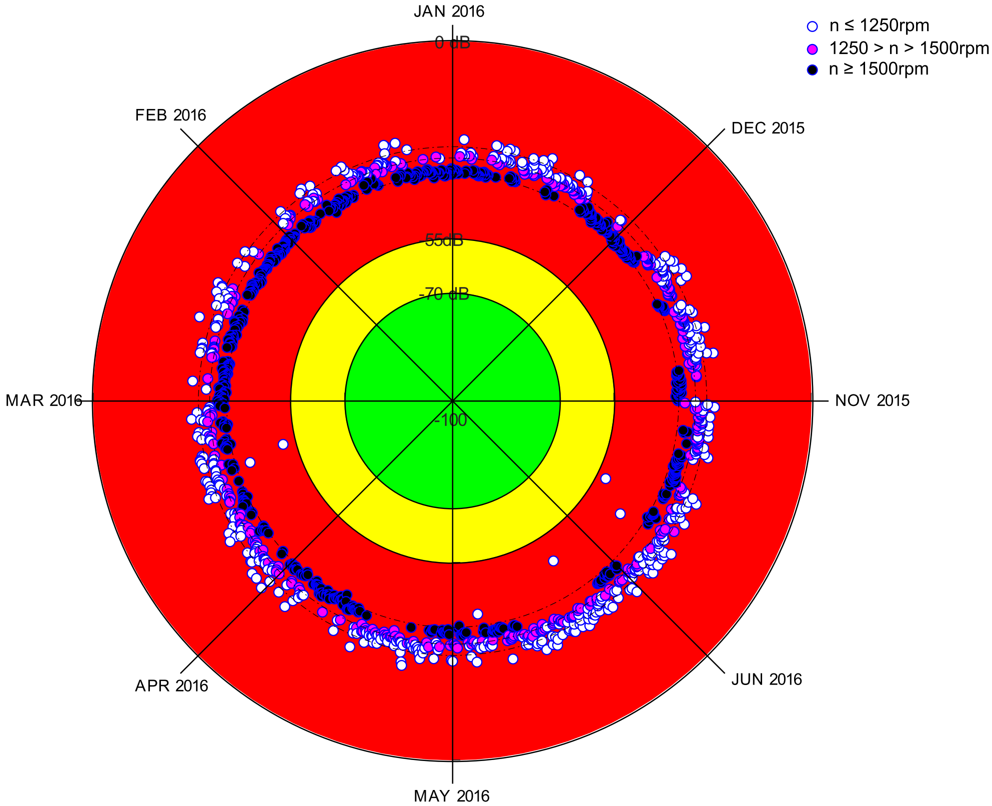

FIGURE 8. **Polar plot of the index *iHota* per date.**

complicating the statistical treatment of the data obtained requiring the individual analysis of each spectrum, a large amount of memory is also required to transfer, process, and store the results. This might limit the application of CSA in the field.

B. THE POTENTIAL OF THE HOTA METHOD FOR CM

Despite the good results of HOTA shown in Section V, the following question can still be posed, *how do loading conditions influence the fault diagnosing results?* To answer this question, further analyses for the whole data-set of the in-service WT DFIG were carried out: one with the data sorted per date of measurement acquisition (see Fig. 8), and another with the data sorted per loading condition (see Fig. 9). A polar plot divided in three colored fault-severity levels was chosen to illustrate these analyses, where the green zone indicates the healthy state, the yellow zone is for incipient faults, and the red zone represents the faulty state. These amplitude levels (in dB) were chosen based on the scientific literature [37].

With this goal in mind, a new index was computed, named *iHota*, corresponding to the average value of the amplitude for $k = -1$ (LSH) and $k = +1$ (USH) fault harmonic components. Three color points were chosen to display the *iHota* index, these being white (for measurements in the *Low* speed range, $\leq 1,250$ *rpm*), purple (for measurements in the *Med* speed range, $1250 < n < 1500$ *rpm*) and blue (for measurements in the *High* speed range, $\geq 1,500$ *rpm*).

Fig. 8 shows the polar plot with the *iHota* values distributed per measurement acquisition date, across the eight months of the monitoring campaign. It can be seen in this plot that the *iHota* values cluster in three different amplitude levels (in dB), where the white points have the highest amplitudes, followed by the purple points, and finally the blue points, which have the lowest amplitude levels. All three levels fall within the red-zone corresponding to the faulty zone. The fact that these three different amplitude levels form three concentric rings, instead of spirals, means that the amplitude levels found across the eight months remain constant, i.e. the severity of the fault does not seem to increase during the monitoring period.

The second analysis, where the *iHota* values are distributed per rotational speed of the DFIG, is shown in Fig. 9. In this plot, it can be observed that the data is now clustered in three speed regimes ($n \leq 1250$ *rpm*; $1,250$ *rpm* $> n > 1,500$ *rpm*; and $n \geq 1,500$ *rpm*) and, hence, in two operating conditions (super and sub-synchronous). The super-synchronous operating condition is formed by blue points (for $n \geq 1,500$ *rpm*) only, whereas both purple ($1,250$ *rpm* $> n > 1,500$ *rpm*) and white ($n \leq 1250$ *rpm*) data points form the sub-synchronous operating condition. It can therefore be concluded that the rotational speed (and thus the operating

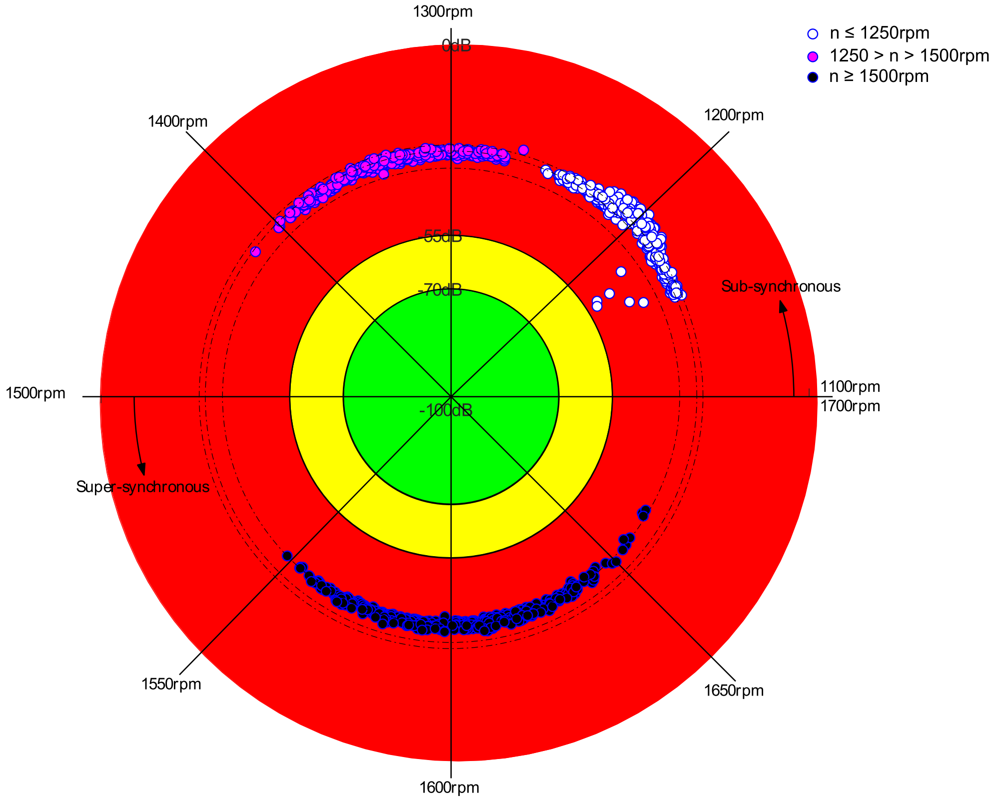

FIGURE 9. Polar plot of the index *iHota* per rotational speed.

condition) has a significant influence on the fault diagnosing results.

VII. CONCLUSIONS

The growing need for WT O&M cost reduction has been amply evidenced. In order to achieve this goal, maintenance strategies must be optimized. The new trends point towards CBM, where CM determines the optimum point between scheduled and corrective actions.

The electric generator is one of the most critical components of WTs. Hence, detection of incipient faults through appropriate CM on this WT component is crucial. However, commercial CMSs fail to achieve this goal. Furthermore, a lack of operational data from in-service WT generators has been identified in the scientific literature. Under this scenario, this study has presented the analysis of an operational WT equipped with a DFIG diagnosed with mixed eccentricity over a period of eight months via the HOTA method.

The HOTA method was developed with two main goals: to facilitate the diagnosis by non-trained maintenance personnel and to reduce the amount of data necessary for the results. A total of 1,285 measurements (for the eight-months period) were analyzed using HOTA. Several graphical representations, as well as statistical analyses, were also carried out. The results show that the method is able to identify and classify the fault related harmonic components (corresponding to mixed eccentricity) in a simple manner, so that large amount of data can be plotted jointly, facilitating the statistical analysis as well as its interpretation by non-trained maintenance personnel.

Furthermore, as this method proposes a simplified representation of the traditional CSA via FFT, the number of data points needed for diagnostic purposes is also reduced to a very small set of data (less than 20 real numbers). As a result, a 99.81% reduction is achieved in the data needing to be stored and transferred (from $1.04 \cdot 10^7$ points to $19,275$ points).

The statistical analyses performed using box plots and color-coded polar plots, show that the amplitude levels of the fault-related harmonic components depend on the loading condition. Hence, by categorizing the data per loading condition, the capability of the HOTA method improves even further, demonstrating its capability for the CM of WTs.

ACKNOWLEDGMENT

The authors would like to thank Ingeteam Power Technology S.A. – UP Service, part of the AWESOME Project Consortium providing the wind turbine data.

REFERENCES

[1] L. Fried, "Global wind statistics 2017," Global Wind Energy Council, Brussels, Belgium, Tech. Rep., Feb. 2018.

[2] A. Honrubia-Escribano, E. Gómez-Lázaro, J. Fortmann, P. Sørensen, and S. Martin-Martinez, "Generic dynamic wind turbine models for power system stability analysis: A comprehensive review," *Renew. Sustain. Energy Rev.*, vol. 81, no. 2, pp. 1939–1952, 2018.

[3] Z. Yang and Y. Chai, "A survey of fault diagnosis for onshore grid-connected converter in wind energy conversion systems," *Renew. Sustain. Energy Rev.*, vol. 66, no. 1, pp. 345–359, Sep. 2016.

[4] Y. Lin, L. Tu, H. Liu, and W. Li, "Fault analysis of wind turbines in China," *Renew. Sustain. Energy Rev.*, vol. 55, pp. 482–490, Mar. 2016.

[5] M. I. Blanco, "The economics of wind energy," *Renew. Sustain. Energy Rev.*, vol. 13, nos. 6–7, pp. 1372–1382, 2009.

[6] Y. Sinha and J. A. Steel, "A progressive study into offshore wind farm maintenance optimisation using risk based failure analysis," *Renew. Sustain. Energy Rev.*, vol. 42, pp. 735–742, Feb. 2015.

[7] J. Ribrant and L. Bertling, "Survey of failures in wind power systems with focus on Swedish wind power plants during 1997–2005," in *Proc. IEEE Power Eng. Soc. Gen. Meeting*, Jun. 2007, pp. 1–8.

[8] F. Spinato, P. J. Tavner, G. J. W. van Bussel, and E. Koutoulakos, "Reliability of wind turbine subassemblies," *IET Renew. Power Generat.*, vol. 3, no. 4, pp. 387–401, Dec. 2009.

[9] G. J. W. van Bussel and M. B. Zaaijer, "Reliability, availability and maintenance aspects of large-scale offshore wind farms, a concepts study," in *Proc. 2-Day Int. Conf. Mar. Renew. Energies (MAREC)*, 2001, pp. 1–9.

[10] Y. Feng, P. J. Tavner, and H. Long, " Early experiences with UK round 1 offshore wind farms," *Proc. Inst. Civil Eng., Energy*, vol. 163, no. 4, pp. 167–181, 2010.

[11] F. Monforti and I. Gonzalez-Aparicio, "Comparing the impact of uncertainties on technical and meteorological parameters in wind power time series modelling in the European Union," *Appl. Energy*, vol. 206, pp. 439–450, Nov. 2017.

[12] P. Hou, W. Hu, M. Soltani, C. Chen, and Z. Chen, "Combined optimization for offshore wind turbine micro siting," *Appl. Energy*, vol. 189, pp. 271–282, Mar. 2017.

[13] M. D. Reder, E. Gonzalez, and J. J. Melero, "Wind turbine failures—Tackling current problems in failure data analysis," *J. Phys., Conf. Ser.*, vol. 753, no. 7, 2016, Art. no. 072027.

[14] J. M. P. Pérez, F. P. G. Márquez, A. Tobias, and M. Papaelias, "Wind turbine reliability analysis," *Renew. Sustain. Energy Rev.*, vol. 23, pp. 463–472, Jul. 2013.

[15] D. Zhang, L. Qian, B. Mao, C. Huang, B. Huang, and Y. Si, "A data-driven design for fault detection of wind turbines using random forests and XGboost," *IEEE Access*, vol. 6, pp. 21020–21031, 2018.

[16] Q. Wei, Z. Pinjia, and C. Mo-Yuen, "Condition monitoring, diagnosis, prognosis, and health management for wind energy conversion systems," *IEEE Trans. Ind. Electron.*, vol. 62, no. 10, pp. 6533–6535, Oct. 2015.

[17] M. J. Kabir, A. M. T. Oo, and N. Rabbani, "A brief review on offshore wind turbine fault detection and recent development in condition monitoring based maintenance system," in *Proc. IEEE Power Eng. Conf. (AUPEC)*, Sep. 2015, pp. 1–7.

[18] J. Carroll, A. McDonald, and D. McMillan, "Failure rate, repair time and unscheduled O&M cost analysis of offshore wind turbines," *Wind Energy*, vol. 19, no. 6, pp. 1107–1119, Jun. 2016.

[19] E. Artigao, S. Martín-Martínez, A. Honrubia-Escribano, and E. Gómez-Lázaro, "Wind turbine reliability: A comprehensive review towards effective condition monitoring development," *Appl. Energy*, vol. 228, pp. 1569–1583, Oct. 2018.

[20] R. A. J. Amalorpavaraj, P. Kaliannan, S. Padmanaban, U. Subramaniam, and V. K. Ramachandaramurthy, "Improved fault ride through capability in DFIG based wind turbines using dynamic voltage restorer with combined feed-forward and feed-back control," *IEEE Access*, vol. 5, pp. 20494–20503, 2017.

[21] N. Ullah, M. A. Ali, A. Ibeas, and J. Herrera, "Adaptive fractional order terminal sliding mode control of a doubly fed induction generator-based wind energy system," *IEEE Access*, vol. 5, pp. 21368–21381, 2017.

[22] B. Lu, Y. Li, X. Wu, and Z. Yang, "A review of recent advances in wind turbine condition monitoring and fault diagnosis," in *Proc. IEEE Power Electron. Mach. Wind Appl. (PEMWA)*, Jun. 2009, pp. 1–7.

[23] W. Qiao and D. Lu, "A survey on wind turbine condition monitoring and fault diagnosis—Part II: Signals and signal processing methods," *IEEE Trans. Ind. Electron.*, vol. 62, no. 10, pp. 6546–6557, Oct. 2015.

[24] M. El Hachemi Benbouzid, "A review of induction motors signature analysis as a medium for faults detection," *IEEE Trans. Ind. Electron.*, vol. 47, no. 5, pp. 984–993, Oct. 2000.

[25] A. Siddique, G. S. Yadava, and B. Singh, "A review of stator fault monitoring techniques of induction motors," *IEEE Trans. Energy Convers.*, vol. 20, no. 1, pp. 106–114, Mar. 2005.

[26] E. Artigao, A. Honrubia-Escribano, and E. Gómez-Lázaro, "Current signature analysis to monitor DFIG wind turbine generators: A case study," *Renew. Energy*, vol. 116, pp. 5–14, Feb. 2018.

[27] E. Artigao, S. Koukoura, A. Honrubia-Escribano, J. Carroll, A. McDonald, and E. Gómez-Lázaro, "Current signature and vibration analyses to diagnose an in-service wind turbine drive train," *Energies*, vol. 11, no. 4, p. 960, 2018.

[28] P. Zhang and P. Neti, "Detection of gearbox bearing defects using electrical signature analysis for doubly-fed wind generators," in *Proc. IEEE Energy Convers. Congr. Expo. (ECCE)*, Sep. 2013, pp. 4438–4444.

[29] F. Cheng, L. Qu, W. Qiao, C. Wei, and L. Hao, "Fault diagnosis of wind turbine gearboxes based on DFIG stator current envelope analysis," *IEEE Trans. Sustain. Energy*, to be published.

[30] A. Sapena-Baño *et al.*, "Harmonic order tracking analysis: A novel method for fault diagnosis in induction machines," *IEEE Trans. Energy Convers.*, vol. 30, no. 3, pp. 833–841, Sep. 2015.

[31] J. Faiz and S. M. M. Moosavi, "Eccentricity fault detection—From induction machines to DFIG—A review," *Renew. Sustain. Energy Rev.*, vol. 55, pp. 169–179, Mar. 2016.

[32] A. Sapena-Bano, J. Burriel-Valencia, M. Pineda-Sanchez, R. Puche-Panadero, and M. Riera-Guasp, "The harmonic order tracking analysis method for the fault diagnosis in induction motors under time-varying conditions," *IEEE Trans. Energy Convers.*, vol. 32, no. 1, pp. 244–256, Mar. 2017.

[33] A. Stefani, A. Yazidi, C. Rossi, F. Filippetti, D. Casadei, and G. A. Capolino, "Doubly fed induction machines diagnosis based on signature analysis of rotor modulating signals," *IEEE Trans. Ind. Appl.*, vol. 44, no. 6, pp. 1711–1721, Nov. 2008.

[34] Y. Gritli, C. Rossi, D. Casadei, F. Filippetti, and G.-A. Capolino, "A diagnostic space vector-based index for rotor electrical fault detection in wound-rotor induction machines under speed transient," *IEEE Trans. Ind. Electron.*, vol. 64, no. 5, pp. 3892–3902, May 2017.

[35] A. Sapena-Bano, M. Riera-Guasp, R. Puche-Panadero, J. Martinez-Roman, J. Perez-Cruz, and M. Pineda-Sanchez, "Harmonic order tracking analysis: A speed-sensorless method for condition monitoring of wound rotor induction generators," *IEEE Trans. Ind. Appl.*, vol. 52, no. 6, pp. 4719–4729, Nov./Dec. 2016.

[36] R. H. Park, "Two-reaction theory of synchronous machines generalized method of analysis—Part I," *Trans. Amer. Inst. Elect. Eng.*, vol. 48, no. 3, pp. 716–727, Jul. 1929.

[37] I. Culbert and J. Letal, "Signature analysis for online motor diagnostics: Early detection of rotating machine problems prior to failure," *IEEE Ind. Appl. Mag.*, vol. 23, no. 4, pp. 76–81, Jul./Aug. 2017.

ESTEFANIA ARTIGAO received the M.Sc. and Ph.D. degrees in industrial engineering from the University of Castilla–La Mancha, Spain, in 2009 and 2018, respectively. Since 2010, she has been with several research entities in U.K., including the University of Birmingham, TWI Ltd., Cambridge, and Brunel University, London, where she involved in the research and development projects within the wind energy sector. Her main research interests include the field of operation and maintenance and condition monitoring of wind turbines.

ANGEL SAPENA-BANO received the M.Sc. and Ph.D. degrees in electrical engineering from the Universitat Politecnica de Valencia, Spain, in 2009 and 2014, respectively, where he is currently an Assistant Professor. His research interests focus on induction motor diagnostics and maintenance based on condition monitoring, numerical modeling of electrical machines, and advanced automation processes and electrical installations.

ANDRÉS HONRUBIA-ESCRIBANO received the degree in electrical engineering from the Polytechnic University of Madrid, Madrid, Spain, in 2008, and the Ph.D. degree in renewable energy from the Polytechnic University of Cartagena, Cartagena, Spain, in 2012. Since 2008, he has been with several research entities. He is currently an Associate Professor with the Department of Electrical, Electronics, and Control Engineering, Castilla La Mancha University, Albacete, Spain. He has published more than 65 articles in journals, books, and specialized conferences as well as collaborating in more than 45 research and development projects. His main research interest includes the integration of wind energy into power systems.

JAVIER MARTINEZ-ROMAN received the Ph.D. degree in electrical engineering from the Universitat Politecnica de Valencia, Spain, in 2002, where he is currently an Associate Professor. His primary areas of interest include electrical machines and drives, and instrumentation systems for electrical installations.

RUBEN PUCHE-PANADERO received the M.Sc. degree in automatic and electronic engineering and the Ph.D. degree in electrical engineering from the Universitat Politecnica de Valencia, in 2003 and 2008, respectively. In 2006, he joined the Universitat Politecnica de Valencia, where he is currently an Associate Professor of control of electrical machines. His research interests include induction motor diagnosis, numerical modeling of electrical machines, and advanced automation processes and electrical installations.

EMILIO GÓMEZ-LÁZARO received the M.Sc. and Ph.D. degrees in electrical engineering from the Universidad Politecnica de Valencia, Valencia, Spain, in 1995 and 2000, respectively. He is currently a Full Professor with the Department of Electrical, Electronics, and Control Engineering, Castilla La Mancha University, Albacete, Spain, where he is also the Director of the Renewable Energy Research Institute. His research interests include the modeling of wind turbines and wind farms, grid codes, power system integration studies, steady-state and dynamic analysis, and the maintenance of renewable energy power plants.